INTEGRATING EXTERNAL HARDWARE ON EXISTING MAGNETIC RESONANCE SYSTEMS FOR COMMERCIALLY UNSUPPORTED APPLICATIONS

A Thesis

by

KURT AARON PARIZEK

Submitted to the Office of Graduate and Professional Studies of
Texas A&M University
in partial fulfillment of the requirements for the degree of

MASTER OF SCIENCE

Chair of Committee,	Mary McDougall
Committee Members,	Alvin Yeh
	Joe Kornegay
Head of Department,	Anthony Guiseppi-Elie

August 2017

Major Subject: Biomedical Engineering

ABSTRACT

Magnetic resonance imaging and spectroscopy provide the potential for breakthroughs in the understanding of disease and evaluation of treatment outcomes in medical conditions such as muscular disorders, cancer, and mental illnesses. Compared to ^{1}H nuclei, secondary (non-^{1}H) nuclei such as ^{13}C, ^{31}P, and ^{23}Na necessitate higher sensitivity detection methods due to smaller concentrations in vivo and intrinsically lower Larmor frequencies. Two ways to increase the sensitivity of experiments using radiofrequency coils are 1) through optimizing the coil size to fit the volume of interest, and 2) through increasing the number of coils over a defined field of view through phased arrays. Clinical scanners are often constrained in these two regards in that the radiofrequency coils available from the vendor are generally much larger than the volume of interest, and clinical scanners are typically equipped with a singular broadband channel. With these limitations, there is a need to extend the capabilities of existing magnetic resonance systems to increase sensitivity for secondary nuclei and for imaging experiments that fall outside the characteristics of a typical human clinical exam (i.e. small samples, animals, or targeted anatomies).

This thesis describes a set of work to address these limitations in order to extend the capabilities of commercial scanners for custom applications. First, the functionality of an existing custom-built multi-channel, broadband receiver is improved through adding calibration capability on each individual channel and through the creation of a user interface that will result in a faster workflow which is critical for live animal

experiments. Second, a custom-built double-tuned coil is interfaced to a 3T clinical magnetic resonance imaging system through a custom built connector, increasing the signal-to-noise ratio for the given application in comparison to the currently available coil for the scanner. Both of these projects work towards integrating external hardware on existing systems to increase the sensitivity of multinuclear studies and customized experiments.

ACKNOWLEDGEMENTS

I would like to thank my advisor Dr. Mary McDougall for her support and education, and for allowing me to pursue the field of magnetic resonance imaging further in my graduate studies.

I would also like to thank my other committee members, Dr. Alvin Yeh and Dr. Joe Kornegay, for their time, interest, and support.

I would like to acknowledge Dr. Steve Wright for the help and knowledge that he has provided through both coursework and in providing access to his facilities. Additionally, thank you to all of the students in Dr. Wright's lab who have helped in this process, especially Jiaming Cui and Stephen Ogier.

I would like to acknowledge all of my family and friends - especially my parents, sister, and Kayla Kehlmann for always supporting and encouraging me.

Lastly, I would like to acknowledge all of my lab mates for always being willing to help and for making graduate school fun. Thank you Romina Del Bosque, Matthew Wilcox, Wen-Yang Chiang, Travis Carrell, Eddie Eigenbrodt, Jeremy Sia, Austin Lu, and Joseph Rispoli.

CONTRIBUTORS AND FUNDING SOURCES

Contributors

This work was supervised by a thesis committee consisting of Dr. Mary McDougall (advisor) and Dr. Alvin Yeh of the Department of Biomedical Engineering and Dr. Joe Kornegay of the College of Veterinary Medicine and Biomedical Sciences.

The 6-channel broadband receiver utilized for research in Chapters III and VI was designed and built by Dr. Edwin Eigenbrodt. The design of the graphical user interface described in Chapter III was performed by Austin Lu, Matthew Kuo, Benjamin Swain, and Victoria Nguyen. Additionally, the *in vitro* preliminary data presented in Chapter IV was performed by Jeremy Sia.

All other work conducted for the thesis was completed by the student independently.

Funding Sources

There are no outside funding contributions to acknowledge related to the research and compilation of this document.

NOMENCLATURE

^{1}H	Hydrogen Atom
^{13}C	Carbon-13 Isotope
^{31}P	Phosphorous-31 Isotope
B_0	Static Magnetic Flux Density
B_1	Radiofrequency Magnetic Flux Density
DMD	Duchenne's Muscular Dystrophy
GRMD	Golden Retriever Muscular Dystrophy
GUI	Graphical User Interface
IF	Intermediate Frequency
LO	Local Oscillator
MRI	Magnetic Resonance Imaging
MRS	Magnetic Resonance Spectroscopy
NMR	Nuclear Magnetic Resonance
PCr	Phosphocreatine
Pi	Inorganic Phosphate
RF	Radiofrequency
TE	Echo Time
TR	Repetition Time
TIPS	Texas Institute for Pre-Clinical Studies

TABLE OF CONTENTS

Page

LIST OF FIGURES

Page

LIST OF TABLES

Page

CHAPTER I:

INTRODUCTION

Magnetic resonance spectroscopy (MRS) has been performed for over 20 years, enabling noninvasive interrogation of ionic and metabolic activity [2]. Such experiments acquire data that would otherwise require invasive biopsy, thereby providing a means to diagnose disease and test treatment outcomes through quantitative measurements without physical discomfort to the patient. MRS has been utilized to better understand various medical conditions, including multiple sclerosis, muscular dystrophy, breast cancer, and cardiac failure [3-6]. The focus of this research specifically is to further the capabilities of acquiring MRS data for ultimate use in the study of Duchenne's Muscular Dystrophy (DMD), as this is the current focus of a set of collaborative studies at the Texas A&M Veterinary School [7].

I.1 Motivation

DMD is a progressive disease that affects 1 in 3600–6000 live male births [8]. DMD's progression leads to widespread skeletal and muscle fiber destruction and connective tissue infiltration. Muscular tissue destruction leads to loss of ambulation as well as cardiac and respiratory complications, which ultimately results in patient's deaths often in their early 20's [8]. There is currently no treatment for the disease, however corticosteroids have proven to prolong the disease progression, and gene therapy is currently being researched as a cure [9].

In evaluating any possible treatment outcome of a disease, it is of extreme importance to provide feedback to the patient so it is known whether or not the treatment is efficacious or if another treatment should be sought. For DMD specially, the gold standard of evaluating treatment outcomes is currently through taking muscle biopsies from patients [8]. This is not ideal, as it puts the patient in discomfort, can be prone to measurement error, and is highly dependent on the disease progression of the muscle biopsied [10]. Clinical testing to evaluate treatment outcomes may be performed, such as having patients physically demonstrate strength and gait, but such tests are difficult to quantify and must be done over a time period of months to determine if disease progression is slowing. Connective tissue infiltration has been viewed through the ability of magnetic resonance imaging (MRI) to induce soft tissue contrast through techniques such as T1-weighted imaging in which fatty tissue appears bright in comparison to muscle tissue [11, 12]. While such imaging methods may provide a comprehensive "snapshot" of the disease severity as an indication of the fatty muscle infiltration, it is difficult to quantify [12]. By contrast, MRS can be utilized as a quantifiable measure of treatment outcomes through measuring the metabolic activity of a particular muscle over time.

MRS studies are of particular interest to the treatment and diagnosis of muscular disorders such as DMD, as phosphorus (^{31}P) can be used to quantify phosphorylated metabolites to gain insight into muscle bioenergetics, hydrogen (^{1}H) to assess lipid content such as connective tissue infiltration, sodium (^{23}Na) to evaluate cellular function, and carbon (^{13}C) to examine glycogen concentrations indicating energy expenditures [2,

13-15]. These nuclei all contribute to form a comprehensive "tissue signature" and provide relevant information relating to the understanding of muscular dystrophy. Therefore, through the application of multi-nuclear studies involving such nuclei, disease progression and treatment outcomes can be better understood without the need to extract muscle biopsies from patients.

I.2 Thesis Chapters and Organization

This thesis is organized to first provide the clinical motivation behind performing this type of research, namely to contribute in ultimately finding a treatment that will cure those affected with muscular dystrophy. Given that MRS is non-invasive and quantifiable, it is viewed as the best option for indicating treatment outcomes. Therefore, the background of what MRS is and how it is performed is then provided. MRS of non-^{1}H nuclei will need maximum sensitivity so that accurate diagnosis may be made, so 2 different ways of increasing sensitivity are described which relate to this research.

The remaining chapters describe the research efforts of this thesis. Chapter III describes the efforts taken to improve the functionality of a custom-made 6-channel broadband receiver. The motivation and resultant graphical user interface are presented, along with the improved capability of being able to calibrate the receiver to maximize sensitivity.

Chapter IV presents the motivation and the design of a connector that interfaces a custom-made coil to a clinical MRI system.

Chapter V exemplifies experiments that were performed which prove the effectiveness of the research efforts presented in the previous 2 chapters. One

experiment performs imaging that previously has never been performed with the custom-made receiver, and the other exemplifies that the connector and accompanying coil accomplish what was set out in designing them in the first place: increasing the signal-to-noise ratio compared to the currently available option.

Chapter VI concludes the thesis with a discussion of the implications that can be made given the research results, along with recommendations regarding future work.

CHAPTER II:

BACKGROUND

II.1 Duchenne's Muscular Dystrophy

DMD is an X-linked inherited neuromuscular disorder due to mutations in the dystrophin gene [16]. It is thought that dystrophin plays an important role in providing mechanical reinforcement to muscle fibers, and therefore, dystrophin could help to protect muscle fibers from potentially damaging tissue stresses developed during muscle contraction [17]. Steroids have been shown to slow the disease progression, but there are currently no known treatments for the disease [18]. With the advent of genetic sequencing, research and clinical trials are currently being performed to test gene therapy as a viable treatment outcome [9].

II.2 Golden Retriever Muscular Dystrophy Model

To better study the progression of DMD and treatment outcomes, animal models have been explored for their similarities to humans both at the cellular level as well as anatomically. Canine X-linked muscular dystrophy shares genetic and morphological similarities to DMD and is considered to be the most useful animal model, with recommendation for it to be the model for future contributions to preclinical study of newly developed therapies [19]. The mouse model appears to be analogous to DMD at the molecular level, however may not be a satisfactory phenotypic model to compare against [20]. The current research of interest related to this project relates to the canine model of the disease, particularly a colony of Golden Retriever Muscular Dystrophy

(GRMD) models and their corresponding controls, of which are bred and cared for in a controlled environment at the Texas A&M Veterinary School under the direction of Dr. Joe Kornegay [21].

The current focus of this research is intended to further the understanding of DMD and treatment outcomes of the disease through examining GRMD canines *in vivo*. The research results of this thesis do not specifically include *in vivo* experiments, rather they demonstrate the ability to increase the sensitivity of such experiments as is necessitated. As indicated in the future work section, *in vivo* experiments with the GRMD models is the next step of this research.

The muscle of interest within the GRMD models which will be analyzed using MRS in the future work of this research is the rectus femoris, one of the four heads of the quadriceps in the pelvic limb of the canine. One of the reasons that the rectus femoris was chosen is that it has a circular shape in the transverse imaging plane, allowing for an attainable region of interest measurement. Additionally, this muscle is also one of the four quadriceps muscles of the human body, allowing for effective translation of these research efforts to similarly performed human studies.

II.3 Continuation of Research to Human Testing

The MR system that was utilized for part this research and that will be utilized in the future of this research is a clinical 3T Siemens Verio scanner. It is capable of performing data acquisition with both canines and humans using the same hardware. Therefore, once proven to be able to accurately assess disease progression and/or

treatment outcomes within the GRMD models, the hardware built for this research may then be utilized for human studies.

Before human studies are performed, the hardware and the subsequent data acquired must prove capable of effectively evaluating disease progression and treatment outcomes on the GRMD models. This will involve comparing the results attained against the current methods of evaluating clinical outcomes within the GRMD canines, namely the six-minute walk test [22]. As the aim of MRS is to effectively provide objective feedback regarding the disease state, a biomarker is sought that will effectively track with the clinical course of the disease similar to the six-minute walk test. While not yet determined, this biomarker will likely involve data acquired from multi-nuclei MRS experiments such as ^{1}H and ^{31}P in order to form a "tissue signature" capable of assessing the disease state.

II.4 Magnetic Resonance Spectroscopy

MRI/MRS is made possible due to the phenomenon of nuclear magnetic resonance (NMR). NMR, discovered independently by Edward Purcell and Felix Bloch, led to their jointly receiving the Nobel Prize in 1952. Breaking the term down, "nuclear magnetic" refers to the intrinsic spin angular momentum of nuclei that contain an odd combined number of protons and neutrons. This property of spin angular momentum results in a moving charge, which creates a magnetic field. Therefore, nuclei that possess an intrinsic spin will act as tiny magnets, as visualized in Figure 1.

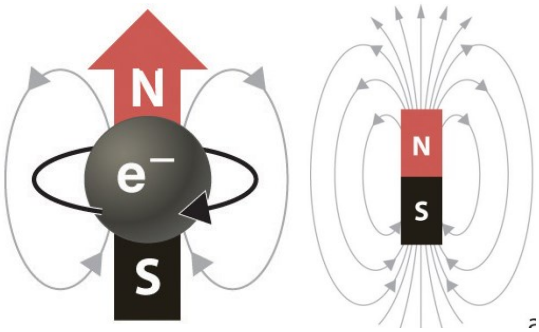

Figure 1: Spin angular momentum results in the nuclei resembling a tiny magnet. Reprinted from [23].

When not exposed to a uniform magnetic field, these spins are randomly oriented and cancel each other out. Once placed inside a uniform magnetic field (B_0), such as within the bore of an MRI scanner, the spins will become cohesively aligned in differing states, with the states determined by the quantum nature of the respective nuclei. For ^1H, which is the most commonly interrogated nuclei for MRI due to its abundance in water and fat, there are two different spin states with which the nuclei orient when exposed to a uniform magnetic field: the for (parallel) or against (anti-parallel) state. The orientation parallel to the uniform magnetic field requires the least amount of energy, so there is a slight excess in this direction. This excess results in a net magnetization in the parallel direction, represented as vector $\bar{M}$ in Figure 2 pointing in the z-direction.

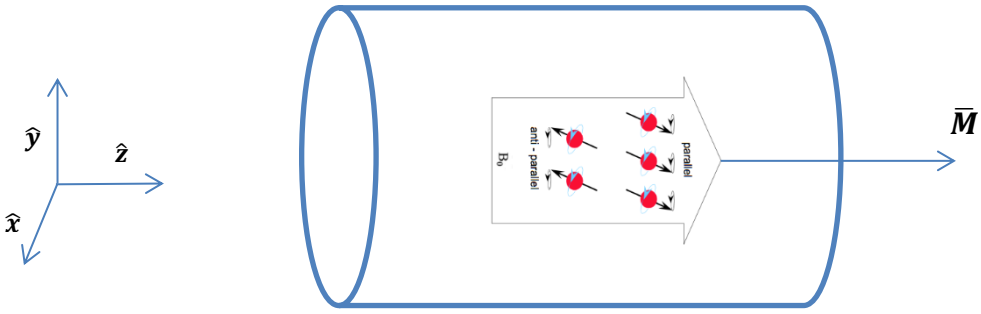

Figure 2: Uniform magnetic field forms a net magnetization vector in the direction parallel to the field

With a slight excess of spins in the low-energy state, there is now an energy difference between the spins in the lower and the higher energy states, known as the Zeeman Effect. This splitting and associated energy difference is visualized in Figure 3, where it can be seen that the stronger the magnetic field strength B_0, the larger the energy difference between energy states.

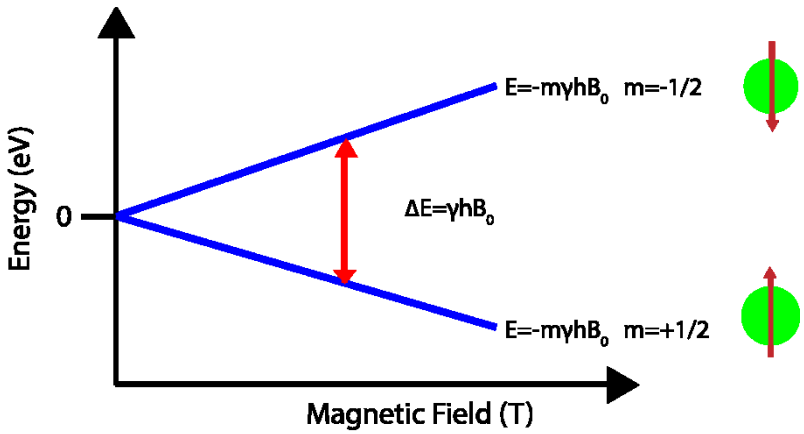

Figure 3: Zeeman effect with spins in two different energy states. Reprinted from [23].

The energy difference between spin states is given by: $\Delta \boldsymbol{E} = \boldsymbol{\gamma h B_0}$, where γ is the gyromagnetic ratio of the nuclei in $\frac{MHz.}{T}$, B_0 is the magnetic field strength in Teslas, and h is planck's constant ($6.62607004 \times 10^{-34}\ \frac{m^2 kg}{s}$). From this equation, Joseph Larmor was able to formulate his Larmor equation $\mathbf{f = \gamma B_0}$, which describes the rate of precession of a nuclei possessing spin angular moment once exposed to a uniform magnetic field. Using the Larmor equation, the energy needed to excite the net magnetization vector can be calculated, dependent on the nuclei that are being interrogated and the magnetic field strength they are exposed to. This explains the third and final term within "nuclear magnetic resonance," with the "resonance" denoting the

absorption of energy at the Larmor frequency. This energy, termed B_1, is produced by a radio frequency coil in an MR experiment and is applied perpendicular to the net magnetization vector, tipping the net magnetization vector into the x-y (transverse) plane. This tipping of the spins is visualized in Figure 4, with the spiral pattern representing the precessing of the net magnetization vector at the Larmor frequency as it is tipped into the transverse plane.

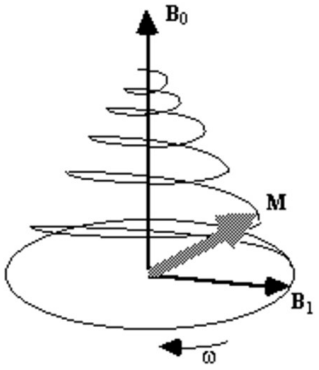

Figure 4: Net magnetization vector tipped into the transverse plane. Reprinted from [24].

Once B_1 has been applied, the net magnetization vector will relax back to equilibrium while still precessing, and induce a voltage across the terminals of an RF coil due to Faraday's law if the coil is tuned to the same Larmor frequency in which the RF pulse was originally applied. This relaxation of the spins, produced by the dephasing of the individual spins between each other, will result in a free induction decay (FID) signal. The Fourier transform of the FID can then be taken, resulting in a spectrum which shows the frequencies the signal was composed of. This transformation may be viewed in Figure 5 below:

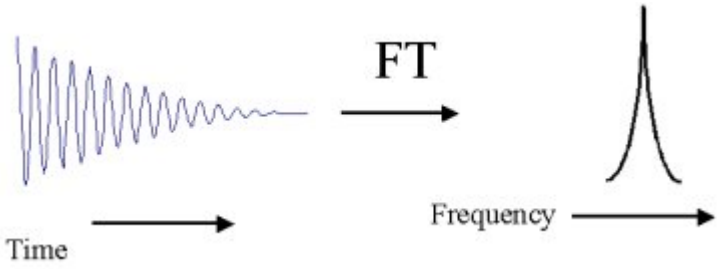

Figure 5: FID acquired and then Fourier Transformed into a spectrum. Reprinted from [1].

This "pulse and acquire" technique is commonly performed in MRS in which the spins of a specified nuclei are excited and then resulting spectra are then analyzed. Nuclei are influenced by their local environments, specifically the electron shells which surround them. Electrons oppose the magnetic field being applied, and therefore shield the nuclei, lowering the frequency at which they become resonant. Electronegativity on the other hand has the opposite effect, increasing the absorption energy for respective nuclei. Shielding will shift the spectra upfield when looking at an NMR spectra, meaning to the right, while electronegativity will shift spectra downfield, meaning to the left [25].

II.5 Magnetic Resonance Imaging

Paul Lauterbur along with Peter Mansfield won the Nobel Prize in 2003 for their discovery of MRI. Paul Lauterbur first applied magnetic field gradients in 1973, allowing for the spatial localization of signals and allowing for the advent of MRI as we know it today [26]. While the focus of this research is to increase the sensitivity for ultimate use in secondary (non-^{1}H nuclei) applications, MRI is performed as part of the research results of this thesis through two different experiments. MRI is able to demonstrate the desired outcomes of this research with the next steps being MRS

experiments. Within imaging experiments, the application of an RF pulse as previously described is still the basis for perturbing the spins, with the only difference in imaging experiments being the application of additional magnetic field gradients which may or may not be applied during pulse and acquire MRS experiments. Through manipulation of imaging parameters and their subsequent effects on the imaging gradients applied, MRI may be utilized to provide the contrast and resolution needed in a wide variety of applications.

II.6 Multinuclear Studies of Muscular Dystrophy

Due to ^{31}P spectroscopy's ability to provide a noninvasive means of quantifying concentrations of key muscle metabolites such as phosphocreatine (PCr) and inorganic phosphate (Pi), phosphorus has been studied since the very earliest of *in vivo* spectroscopy studies [2]. Such studies have performed to gain insight into muscular dystrophy in humans and canines alike. In humans, ^{31}P spectroscopy has been able to detect impaired muscle energy metabolism, as evident from the decrease in the ratio of PCr to adenosine triphosphate (ATP) [27]. Such a result is indicative of a loss in contractile tissue [28]. In canines, McCully noted that during stimulation, the Pi to Pcr ratio was normal compared to the control in diseased canines, but 2 to 3 days after stimulation, the ratios were significantly increased in the diseased canines compared with the controlled, non-diseased canines who showed no increase following rest [29]. The elevated Pi/PCr ratio reflects higher ADP levels at rest, which in turn reveals a dysregulation of the mitochondrial oxidative phosphorylation control and/or an abnormal energy demand to maintain ionic homeostasis despite leaky cell membranes [28]. Wary

et al. found a characteristic splitting of the Pi peak within the diseased spectra of canines, and reinforced the similarities found between the canine and human diseased spectra further verifying their comparison in the study of the disease [28].

Beyond ^{31}P, there are also additional nuclei that have proven to be effective in quantifying diseases that affect the muscles, such as ^{1}H, ^{23}Na, and ^{13}C. As muscular dystrophy is a disease characterized by the replacement of muscular tissue by fatty connective tissue, ^{1}H MRS can be utilized to assess lipid content. For instance, ^{1}H MRS has been proven to be useful as a method to quantify intramuscular lipid concentrations in muscular dystrophy patients [7]. Studies have also revealed that the ^{23}Na concentration, meant to evaluate cellular function, is significantly higher than that of healthy subjects in the calf muscles of muscular dystrophy patients. Higher than normal sodium concentrations may be indicative of infiltration of the extracellular sodium and is able to determine disease severity [14]. While ^{13}C MRS may be used to examine the glycogen concentrations in muscle, there is not a known MRS study has been done in order to analyze ^{13}C in DMD patients. Regardless, in a study analyzing muscle glycogen metabolism invasively in mice, it was found that the absence of dystrophin leads to alterations in glucose metabolism in both skeletal muscle as well as liver tissue [15]. All of these nuclei are relevant to the study of DMD, and therefore each will be studied in the future work of this research in order to form a comprehensive view of the disease using MRI/MRS experiments.

II.7 Second-Nuclei Sensitivity

MRS is often performed through a double-tuned coil with one of the two frequencies being ^{1}H, allowing scout imaging to determine correct coil placement for optimal anatomical spectroscopy acquisition, or when dealing with nuclei such as ^{13}C, allows for the decoupling of chemical bonds [30]. Therefore, an emphasis within the experiments performed for this research project will be double-resonant structures. For all of the experiments, surface coils are utilized as the receive elements, with coils placed adjacent to a region-of-interest (ROI) of a NMR-active sample. Surface coils were chosen as the receive elements due to the need to optimize the signal-to-noise ratio (SNR), with the form factor of the coils made to fit the ROI [31]. The coil, if much larger than the muscle of interest, introduces unnecessary noise, causing a decrease in SNR, motivating the need for coils customized to interrogate specific models. Radiofrequency excitation will utilize either volume coils, represented as birdcage or saddle coils, or surface coils which will then act as both the transmit and receive coils. Clinical imaging is primarily performed through interrogation of ^{1}H, due to the abundance of protons within a patient's body. The same abundance cannot be utilized for other secondary (non-^{1}H) nuclei, with the sensitivity of secondary nuclei being much lower. Shown below in Table 1 is a comparison between ^{1}H and the secondary nuclei which have been discussed as being of interest to muscular dystrophy studies thus far: ^{31}P, ^{23}Na, and ^{13}C.

Table 1: Sensitivity of secondary nuclei compared to hydrogen

Nuclei	Gyromagnetic Ratio ($\frac{MHz.}{T}$)	$\frac{\gamma_x}{\gamma_{1H}}$	Natural Abundance	Relative Sensitivity
^{1}H	42.57	1	99.9%	1
^{23}Na	11.26	0.26	100%	1.8
^{31}P	17.24	0.41	100%	6.9
^{13}C	10.71	0.25	1.1%	1.6

It can be seen that ^{31}P has the highest sensitivity out of the three secondary-nuclei which are presented, however it is still much smaller than ^{1}H. Beyond having coils better fit the region of interest to increase sensitivity as previously discussed, arrays of surface coils also provide the ability to increase sensitivity of experiments and are currently an active area of research focus in the field of MRI [5, 32, 33]. These two options: building coils that better fit the region of interest and utilizing array coils will be the focus of this work on increasing the sensitivity in second-nuclei applications.

CHAPTER III:

INCREASING THE FUNCTIONALITY OF A CUSTOM-BUILT BROADBAND RECEIVER

III.1 Custom-Built Receiver

Arrays of receive coils may be utilized in order to increase the sensitivity of MRI and MRS acquisitions. For arrays of receive coils, the multiple coils must be combined onto a single channel or multiple independent receive channels are needed to account for each of the coils. Ideally, a channel per coil would be available to allow for independent gain adjustment between channels if needed. However, it is highly unusual for scanners to be equipped with broadband multi-channel receivers due to cost and complexity. For instance, the commercial scanner at the Texas Institute for Pre-Clinical Studies (TIPS) has 32 receiver channels for receiving ^{1}H, but only a single broadband receiver channel capable of receiving data for non-^{1}H experiments. A custom-built 6-channel broadband receiver has been constructed in order to extend number of broadband channels on such systems [33]. The purpose and utility of this multi-channel, multi-nuclear receiver is that, utilizing hardware that is both inexpensive and portable, it can acquire multiple channels of any frequency of interest up to a 7T. The system can then be utilized on systems such as the one at TIPS, providing tremendous potential for extending the capability of such imaging systems in allowing for multi-nuclear array coils to be utilized. As is, the set-up and operation of the receiver is perplexing and requires expertise of the system. Such complexity increases the amount of time for each

experiment and decreases the receiver's workflow capability, which is of vital importance especially when imaging live animals. To aid in the workflow of the receiver, a graphical user interface (GUI) has been constructed that greatly simplifies the process of acquiring data.

III.2 Building Graphical User Interface

The current configuration of the receiver involves multiple programs, with some written in C and accessed through the command line interface and the rest separately accessed within MATLAB, with each requiring the separate input of similar variables. Figure 6 gives an overview of the files and their respective inputs that currently must be configured. This project involved taking these multiple computer programs, each of which currently requires inputs separately, and forming a Graphical User Interface (GUI) in which all available inputs will be aggregated within a single organized user interface. As part of the GUI and as an improvement to the project, a calibration option was also built into the GUI so that the user is able to account for the different loads that differing coils may experience within an experiment. Immediately upon scan completion, the user is able to be presented the images or spectra that have been acquired as they are processed from the raw data. Upon viewing these, the user may then either save or clear the data.

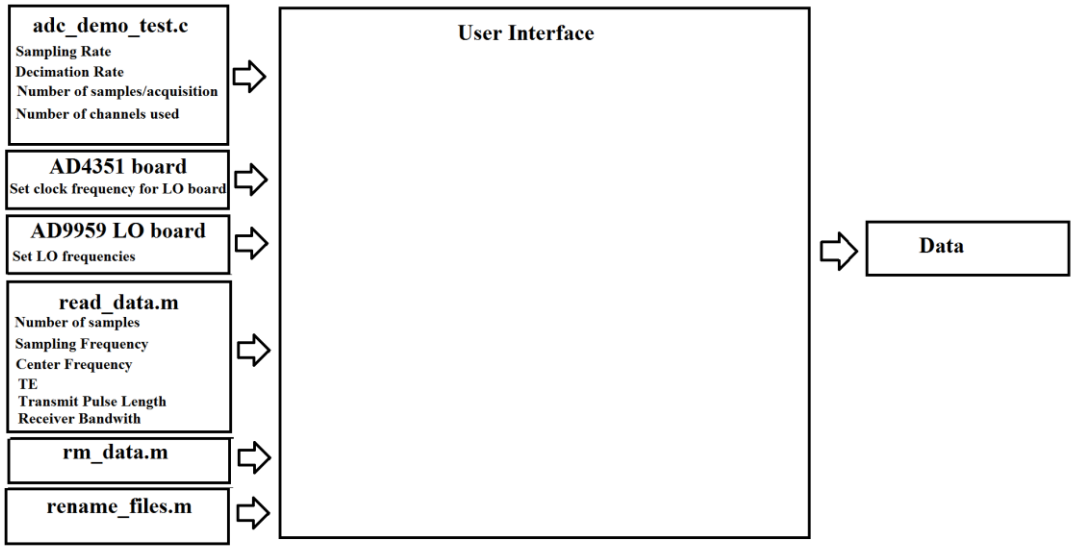

Figure 6: Overview of the previous input files needing configuring and how they all will go into a user interface

Seen below is a picture in Figure 7 of the portable receiver built by Dr. Edwin Eigenbrodt [33]. It can be seen that there is a large custom-built computer and corresponding monitor, a small laptop, and then the other parts of the receiver below those on the bottom of the cart. The top-most aluminum box on the bottom consists of the power supplies needed to power the electronics, the one below that contains the local oscillator generation board needed to drive the mixers for each of the 6 receive channels, and each of the three bottom silver boxes below that correspond to a single intermediate frequency (IF). Each channel uses a heterodyne-style circuit, which is dependent on the frequency being received as well the local oscillator (LO) frequency for that channel which is set within the interface of a program on the small laptop. Once the receiving system has been powered, the first two software programs that are configured are on the small laptop to set the local oscillator frequencies. The small laptop is utilized, as the

desktop runs on a Linux operating system and the drivers for the boards needed to set the LO frequencies are only capable of being run on a Windows operating system. The first two of these programs is for a AD4351 clock frequency board (Analog Devices, Norwood, MA), and it is used to set a stable 500 Megahertz clock for the local oscillator board. Next is the program for the AD9959 local oscillator board (Analog Devices, Norwood, MA) which sets the local oscillator frequencies selected by the user. Once these are set, the ICS-1650A digitizer card (Abaco Systems, Huntsville, AL) must be configured, performed through the command line of the larger custom-built computer. Each experiment may be different, so variables within the adc_demo_test.c including the sampling rate, the decimation rate, the number of samples to take per acquisition, and the number of channels needed must be changed. Once configured, the adc_demo_test.c program is compiled, and the experiment can then be performed. The digitizer is triggered with each acquisition through specially run pulse sequences on the corresponding MRI system, with each acquisition corresponding to a line of k-space if it is an imaging experiment, or a single spectra if spectroscopy is being performed. Once the experiment is completed, MATLAB is opened, allowing for the data to be processed and viewed. Upon reviewing the data, if it is unsatisfactory for any reason, the experiment must be run again and the same process followed.

Figure 7: Portable Frequency-Agnostic Receiver

A GUI was written to consolidate this process and the number of files that need manipulating prior to and during experimentation. Special thanks goes to undergraduates Austin Lu, Matthew Kuo, Benjamin Swain, and Victoria Nguyen who all contributed to the design and coding of this user interface.

The GUI was chosen to be written within MATLAB, as MATLAB is already utilized on the computer for post-processing. Upon opening MATLAB and running the program containing the GUI, the first tab the user is presented with instructs the user how to set up the programs running on the small laptop as seen in Figure 8:

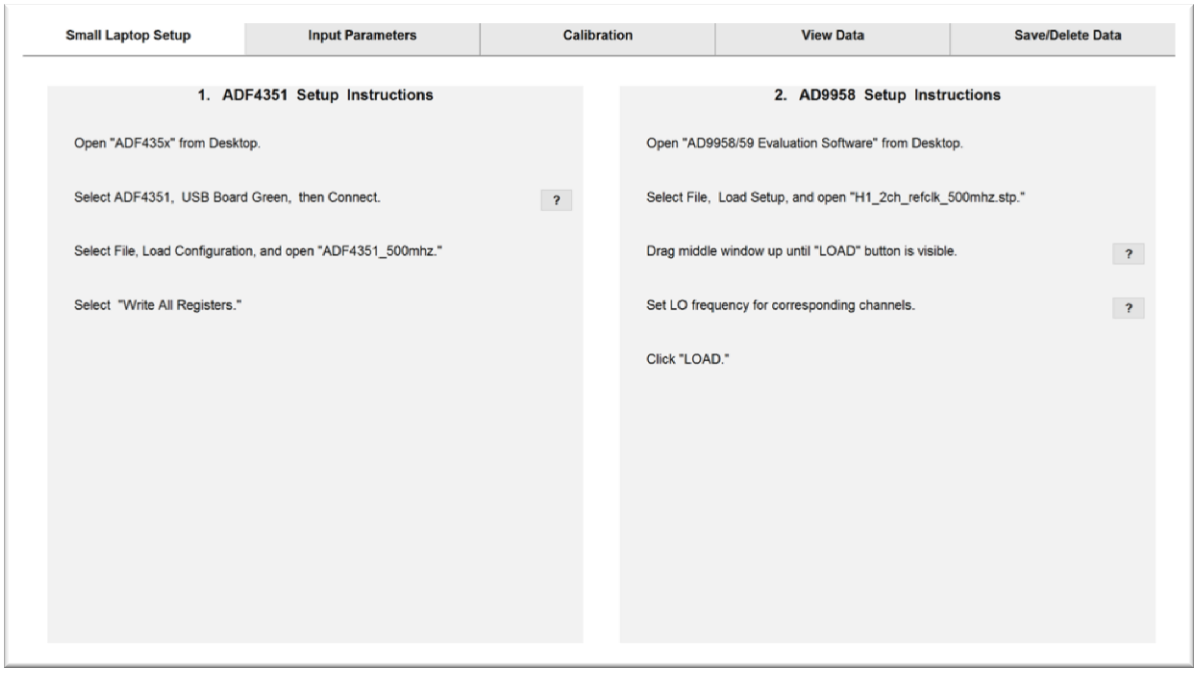

Figure 8: First Tab of GUI - Explaining the Small Laptop Setup

Upon the small laptop being set up, the user may then move on to the next tab, seen below in Figure 9, in which they will input the parameters for the adc_demo_test.c file. Hitting 'Submit Parameters,' MATLAB will find the file in respective directory it is assigned to, and the system will compile the code. This was a task that previously involved opening the program before each experiment and compiling the program each time on the command line. With the parameters entered, the experiment may then be run.

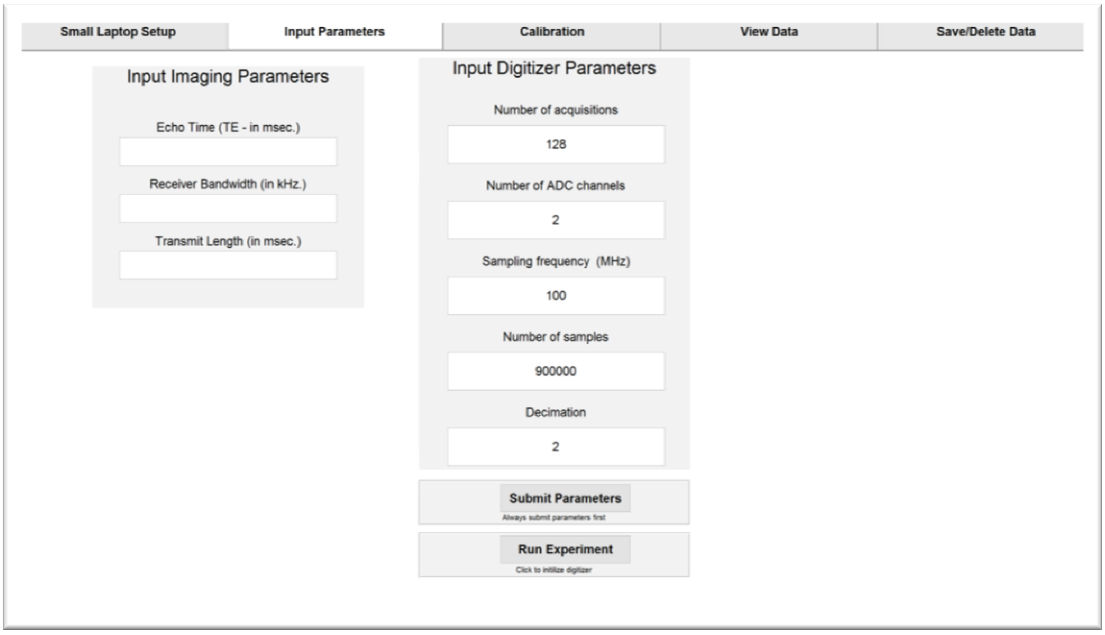

Figure 9: Second Tab of the GUI - Allowing for the Input of Parameters for the Digitizer

The receiver, capable of acquiring data of nuclei at magnet field strengths up to 7T, is also capable of receiving data at many different power levels. This allows for the receiver to obtain signals from coils that either do or do not have pre-amps attached to them. While the receiver does have amplifiers incorporated to increase the signal strength of the inherently low MR receive signals, if presented with data from coils that already have pre-amplifiers, the system will therefore be overloaded and data clipping will occur. The largest signal amplitudes in an MRI experiment occur at the center of k-space which represents the low spatial frequency data, and data clipping will therefore interfere with image contrast. If the opposite occurs and if the receiver attenuation is set too high, then receiver gain will be insufficient, and the image noise will increase as a result of the lower SNR. The images below, obtained on the receiver through imaging

with Wen-Yang Chiang's 6-channel array mouse coil exemplifies the effect of having too low compared to the optimized attenuation level [32]. The images were acquired, taken axially with a homogenous circular phantom meant to imitate the loading that would be presented with a live mouse. Note that in Figure 10, signal can be seen outside of the phantom, representing an overflow "halo" artifact, while in Figure 11, all of the signal is contained within the phantom itself allowing for comparably deeper penetration of signal given the same transmit pulse strength.

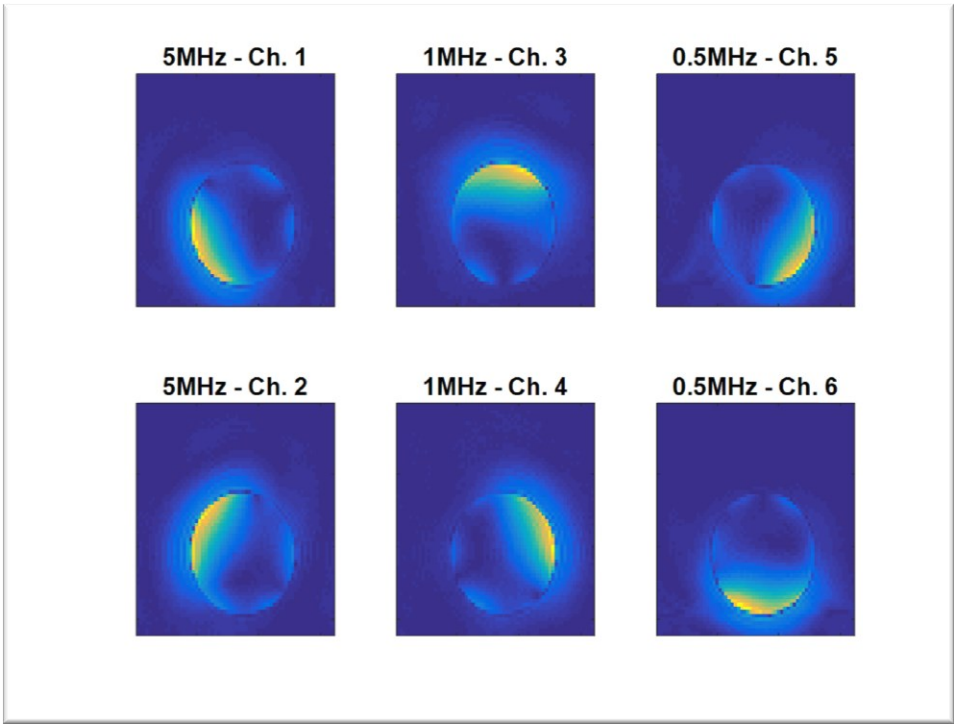

Figure 10: Receiver Overload Artifact - Exemplifying the Importance of Calibration

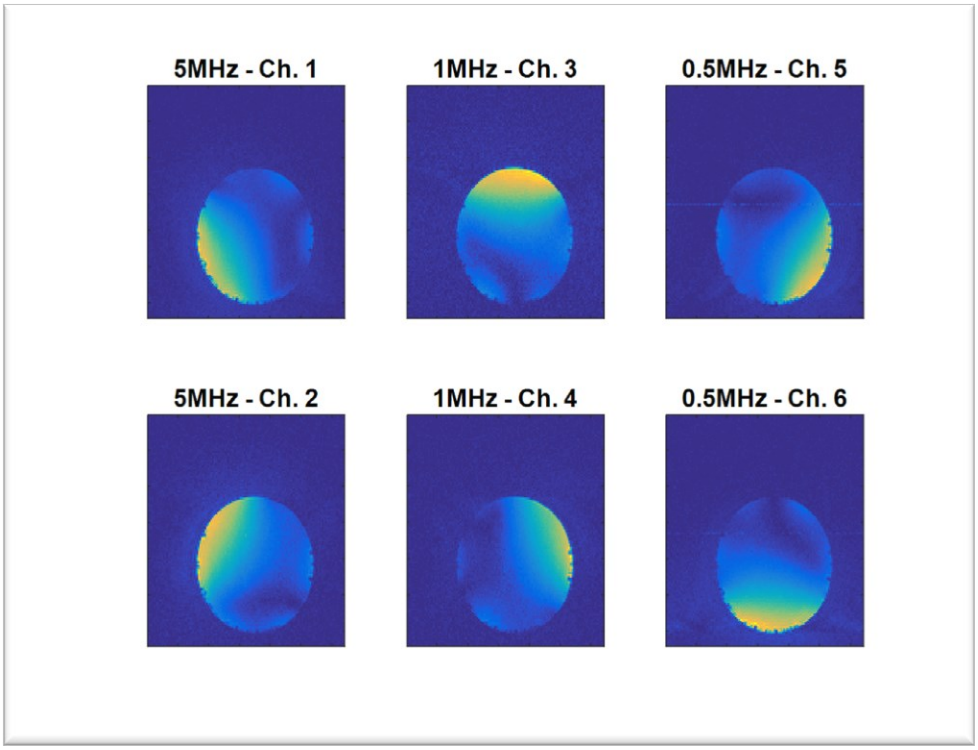

Figure 11: Image with the Artifact Gone - Following Proper Calibration

To account for the large differences in signal strength that the receiver may be exposed to, each channel contains a ZX73-2500+ variable attenuator (Mini-Circuits, Brooklyn, NY). The control voltage of the attenuator was previously adjusted via a bulkhead mounted potentiometer that could vary the control voltage from 0-5 V. As will be discussed, this linear potentiometer was replaced by a logarithmic potentiometer due to the non-linear nature of the attenuator.

Previously, whole experiments were run and the resultant data interrogated in order to check for saturation, but this is time consuming and cumbersome. Therefore, a calibration function has been built into the GUI, seen below in Figure 12. The setup for the calibration is the same as a normal experiment, except instead of going through all of

the lines of k-space and then producing an image, the system is continuously "pinged" through a pulse and acquire sequence implemented on the native console with no gradients applied, allowing for the maximum amount of signal to be received. An attachment has been added to the attenuation knob to represent the attenuation numerically through numbers that go from 1 to 10, with 1 being the highest amount of attenuation and 10 being the lowest. Note that the knob will need to be moved manually between data acquisitions. Seen below is an example of this application being applied as part of an experiment. In each of the respective acquisitions from 1 to 6 (representing each of the 6 receiver channels), the initial "block" of signal is the part of the transmit signal and can be ignored, as it is picked up in order to allow for phase correction in the post-processing step. Following the transmit pulse, it can be seen that the echoes continually increase until a maximum value is reached. The maximum value represents the point at which the receiver is overloaded. The discrepancy between the ranges given by the first 3 plots compared to those thereafter is attributed to the nonlinearity of the attenuator. A logarithmic potentiometer has therefore been added instead of the previous linear potentiometer in order to allow for an increase in linearity in attenuation, thereby allowing a better comparison and ultimate decision on attenuation level. This calibration procedure is performed on each of the channels that will be used for the respective experiment, allowing for the sensitivity of the coil presented by its current load to be accounted for and producing optimal results for each coil. It was found through trial and error that for optimal attenuation, that the echo amplitude must be approximately 70% of

the transmit signal represented by the first block of signal. All channels which are being utilized for an experiment should aim for this metric.

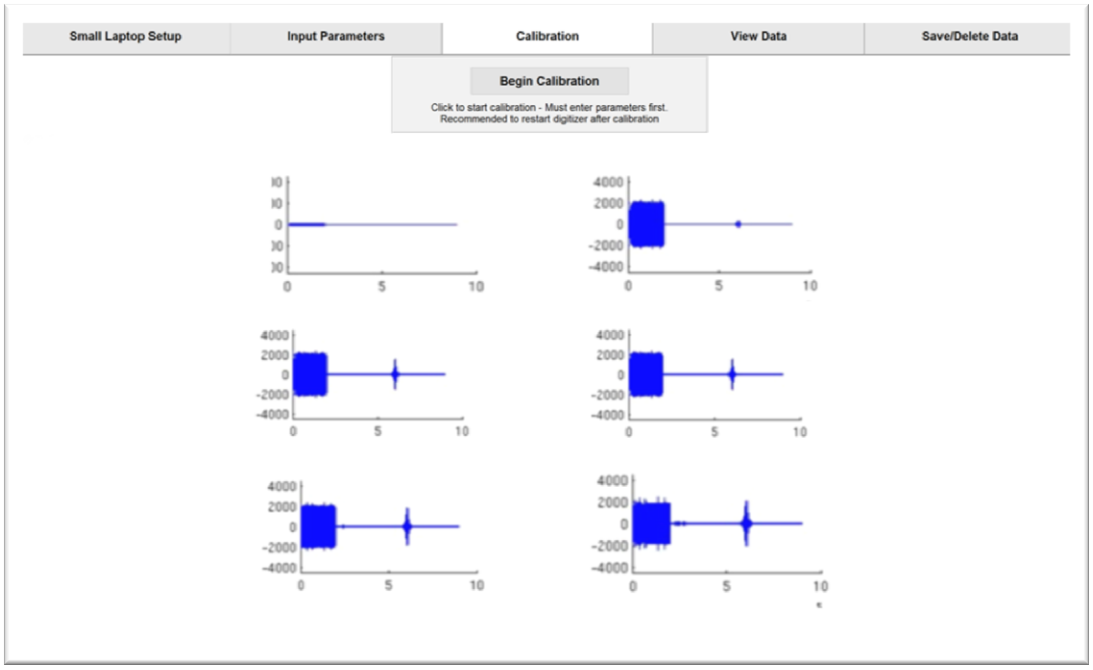

Figure 12: Tab 3 of the GUI - Calibration Example

Once calibrated, the user may then run their respective experiment. The scan must be initiated on the local console of the MR system being used, but through triggers that are connected to the local system which notify the digitizer when to start acquiring data, the process of acquisition requires no further user input. Once the experiment is complete, the user can go to the 'View Data' tab seen below in Figure 13 in order to view the data from each of the channels where acquisitions were acquired. The user enters the imaging parameters that were chosen into the inputs of the GUI at the very beginning. Before, this had to be done manually each time into the respective MATLAB processing

file.

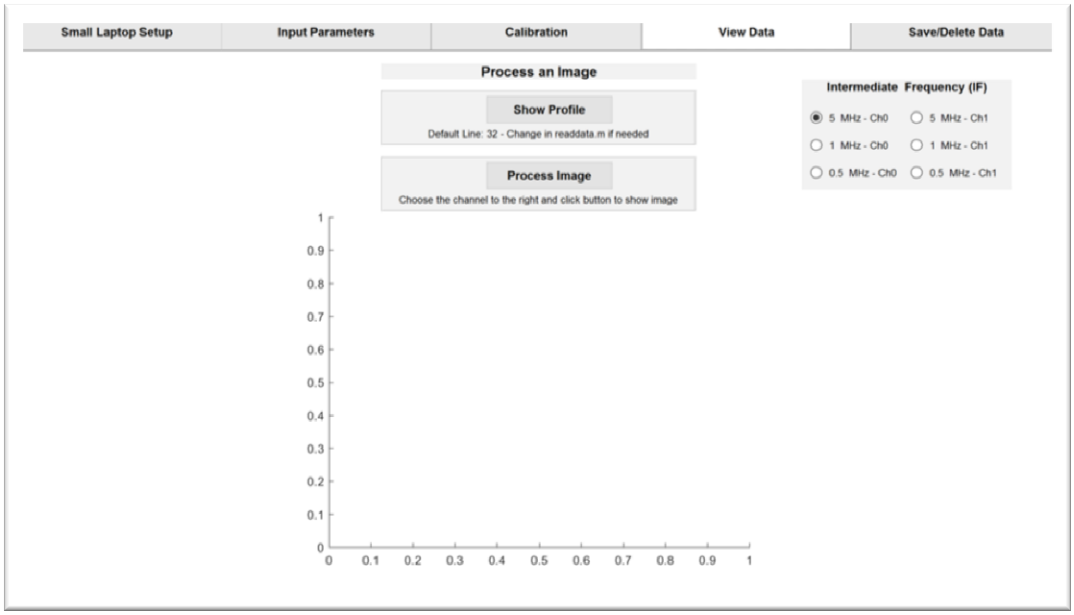

Figure 13: Tab Four of the GUI - Exemplifying Post-Processing

If the user is satisfied with the data, they may then save the data within the 'Analyze Data' tab through renaming the files, seen in Figure 14. If not satisfied, the user may then remove the data, clearing the memory for the next acquisition.

Figure 14: Tab Five of the GUI - Allowing for the user to Save or Remove the Data

With the GUI complete and calibration implemented, it was then utilized in order to image a live mouse. While the receiver was capable of doing this before, the GUI and subsequent improved helped greatly in being able to image the mice.

CHAPTER IV:

CUSTOM-BUILT CONNECTOR

IV.1 $^{31}P/^{1}H$ Butterfly/Loop Commercial Coil

The Texas Institute for Preclinical Studies (TIPS), which works closely with the Texas A&M Veterinary school, owns a 3T Siemens Verio MRI system which is utilized for a variety of studies including those involving the GRMD canines previously discussed. The MRI system itself came equipped with a set of commercial coils, including a butterfly/loop coil which transmits and receives ^{1}H with the butterfly coil and ^{31}P with the smaller loop. This coil measures approximately 20x30 centimeters, as represented by the large blue coil to the left in Figure 15.

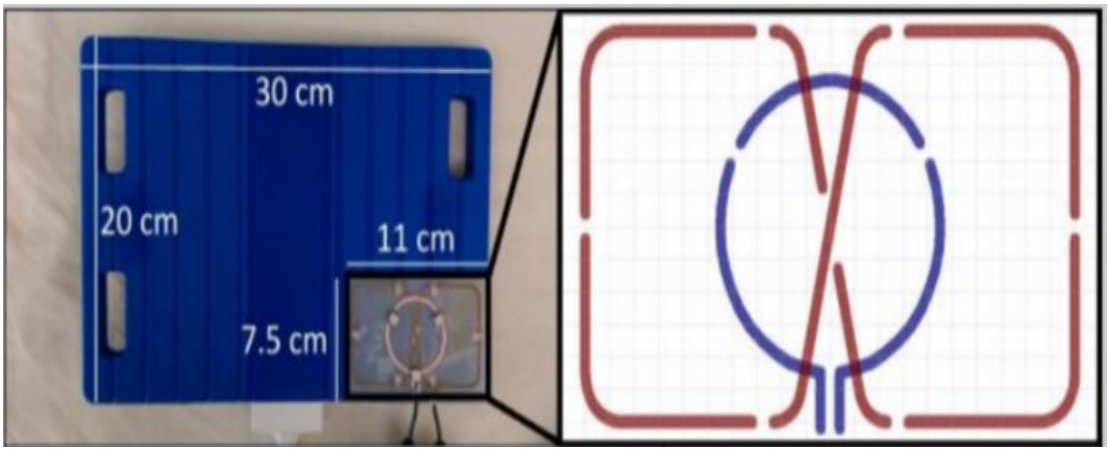

Figure 15: Commercial Coil vs. Custom-Built Coil.
Reprinted from [34].

In order to maximize sensitivity, surface coils should be designed in order to fit the volume of interest as best as possible. Coils that exceed optimal size will acquire excess noise in addition to the signal, resulting in a lower SNR than if the coil was

optimized for the respective volume. It has been shown that for a loop coil to stay within 90% of the optimum SNR, it should be designed such that $0.25 \leq \frac{R}{y} \leq 0.70$, where R is the coil radius and y is the depth of the target region, both in centimeters [35]. The muscle of interest in the current study is the rectus femoris, located at a depth of approximately 2 centimeters on one of the four heads of the quadriceps in the pelvic limb of the canine. The size of the commercial coil is much too large for such an application, and therefore would contribute excess noise in comparison to a smaller coil designed to fit the volume of interest more precisely. As discussed previously, in dealing with ^{31}P spectroscopy experiments, SNR must be maximized due to the inherently lower available signal of the ^{31}P compared to ^{1}H. Therefore, a smaller coil was built using the same ^{31}P/^{1}H butterfly/loop configuration specifically for the application of interrogating the GRMD canine models. This is the coil which can be seen in comparison to the larger commercial coil Figure 15 above.

IV.2 Custom-Built Connector

With the coil built, a custom-built external connector is still needed in order to interface with the clinical system, as you cannot directly connect to the Siemens clinical scanner using a generic type of connection such as conventionally utilized for most MRI research scanners such as BNC or SMA. Rather, a specialty made connector is needed for the system. Along with the larger commercial coil, a corresponding interface box is also required in order to be able to transmit and receive for ^{31}P and ^{1}H independently, which can be seen in Figure 16. According to the Siemens documentation, the interface box contains a diplexer, transmit/receive (T/R) switches, and pre-amps to transmit and

receive both the $^{31}P/^{1}H$ signals separately from the respective coils. Options for connecting the custom-coil to the clinical system include either building another interface box which would be very similar to the commercial equivalent but with a different resistor values indicating a different coil to the system, or creating a connector that would allow for the custom coil to connector directly to the interface box. While the option of creating an interface box would allow for additional customization in that the coil files which set parameters such as the minimum and maximum transmit power requirements, as can be seen in Table 2, the cost would far exceed that of building a connector. Knowing that the larger commercial coil requires far more power than the smaller custom coil, the only concern in building a connector rather than a whole new interface box and corresponding coil files is whether or not the power could be manipulated to be low enough in order to receive data with over-tipping of the respective spins.

Figure 16: Interface box which corresponds with the $^{31}P/^{1}H$ commercial coil

Table 2: Price comparison between new interface box and new connector

Interface Box			Connector		
Parts	**Cost/Part**	**Total**	**Parts**	**Cost/Part**	**Total**
2 Cables	$1,000	$2,000	4 Resistors	$0.10	$0.40
2 Pre-amps	$100	$200	2 BNC Connectors	$5.00	$10.00
2 T/R Switches	$50	$100	3-D Printing	$10.00	$10.00
Miscellaneous	$100	$100	Male Connector	$11.00	$11.00
	Total	$2,400		Total	$31.40

The connector was chosen due to the much lower cost and overall simplicity. In building the connector, the first consideration was how the system would actually recognize the coil. Provided within the Siemens documentation is information indicating that different values of resistors on a coil must be utilized across specific pins, whose values are then converted and read by the scanner has a hexadecimal "coil code." Given that the custom coil was meant to be recognized by the system as the commercial coil but then with the intention to change the minimum power levels, the resistor network was made to match that as measured on the commercial coil. In designing the connector, it needed to be able to fit into the slot that the current connector fits into while also being able to hold the resistor values necessary for the coil to be recognized by the commercial system. The connector was designed in CAD software and then 3D-printed. The CAD designs and printed parts including the resistors can be seen below in Figure 17:

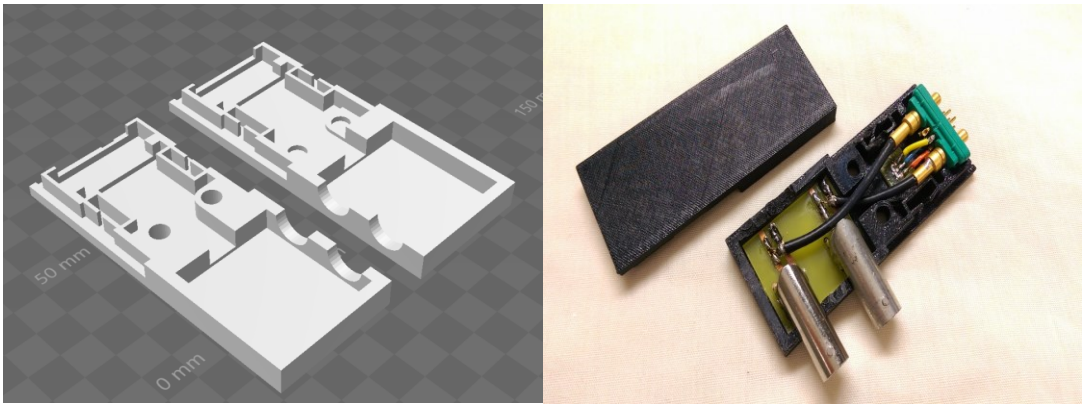

Figure 17: Connect designed in AutoCAD and then 3-D printed

Lastly, seen below in Figure 18 is a picture of the connector that is used for the commercial coil (left) next to the completed custom-built connector (right). It can be seen that the connectors look very similar.

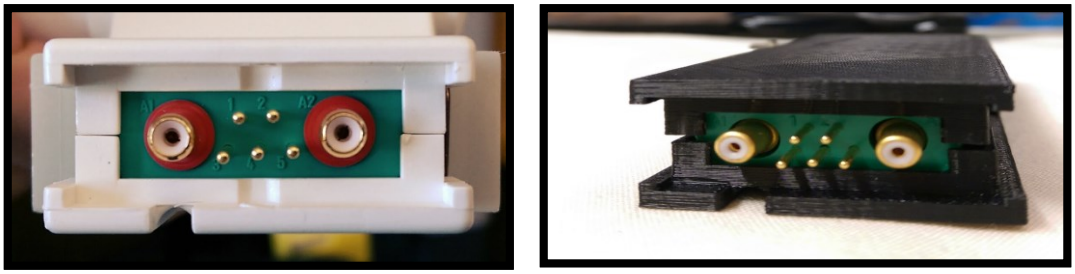

Figure 18: Connector on commercial coil and corresponding 3-D printed connector meant to replicate it

IV.3 Preliminary Testing

Preliminary imaging and spectroscopy experiments were performed *in vitro* with a custom-built butterfly/loop coil by Jeremy Sia on a 4.7T Varian INOVA system of the same size as would be utilized at 3T. Experiments were performed on a physiologically modeled phantom of 20 mM Pi and on pectineus muscle samples of the GRMD canine

population at various stages of disease along with a controls of the same species [34]. ^{31}P spectra obtained from all pectineus muscle samples are shown below in Figure 19, with the volume normalized by fluid displacement measurements. It can be seen that with the GRMD group (represented by red), as age increases, the amplitude of the phosphocreatine peak decreases. Additionally, the control (represented in blue), has a higher phosphocreatine amplitude than comparably aged GRMD samples.

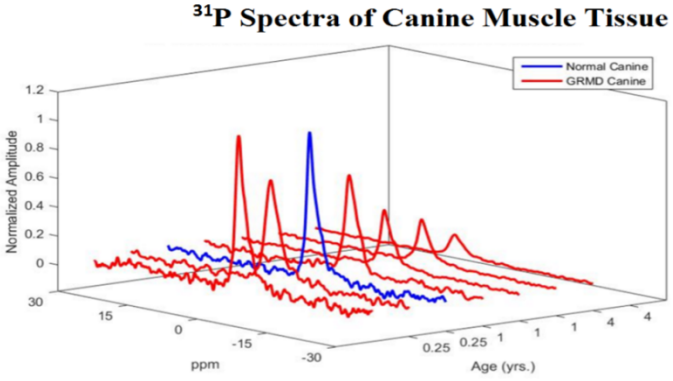

Sample	Age (Years)	Integral Under Curve
1	0.25	72.71
2	0.25	68.30
3	1	69.88
4	1	54.74
5	1	34.89
6	4	24.44
7	4	14.41

Figure 19: Preliminary Experiment performed at 4.7T on Canine Muscle Samples. Reprinted from [34].

While only the phosphocreatine peak is visualized, these results, as expected, show similar results previous ^{31}P studies on muscular dystrophy within the literature previously mentioned which indicate that PCr decreases with disease severity, in this case indicated by the age of the GRMD models [27]. With the connector complete and the coil proven to be effective at obtaining ^{31}P spectra, it was then utilized in an experiment to prove its functionality through imaging a phantom on the 3T Siemens Verio scanner at TIPS.

CHAPTER V:

MAGNETIC RESONANCE IMAGING EXPERIMENTS

V.1 6-Channel Array Live Mouse Imaging Simultaneous Acquisition

This first experiment demonstrates the increased workflow of the receiver, performing an imaging experiment on a live animal which had previously not been attempted with the receiver. The experiment involved the imaging of an anesthetized mice using a 6-channel surface coil array that is paired with a shielded birdcage for the transmit coil, built by Wen-Yang Chiang, as can be seen below in Figure 20 [32]. The handling of the mice was performed by approved students within Dr. Vincent Gresham's laboratory of the Texas A&M Veterinary School. Given that these are anesthetized animals, time is of utter importance in ensuring their safety. Therefore the calibration process built into the GUI proved extremely important in being able to quickly account for the sensitivity of each coil followed by using the GUI to aid in the workflow much better than previously be achieved.

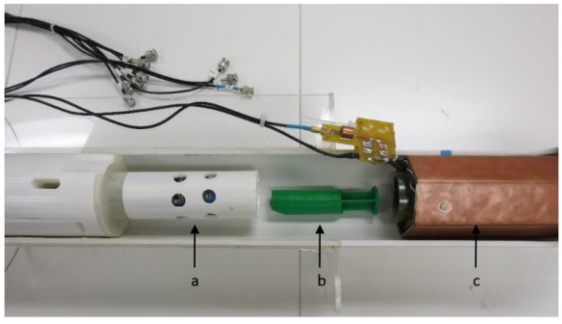

Figure 20: 6-Channel Array and Transmit Coil -
a.) receive coils b.) phantom used previously c.) birdcage

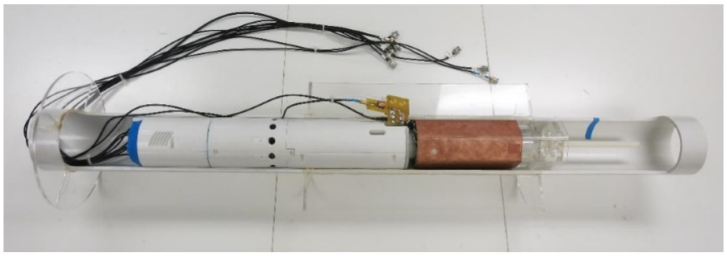

Figure 20 : Continued

Seen below in Figures 21 and 22 are the resultant images from each of the 6 coils of a mouse brain along with the combined image, combined using the sum of squares method. These images were taken with an echo time (TE) of 20 msec. and a repetition time (TR) of 800 msec. using a spin echo pulse sequence.

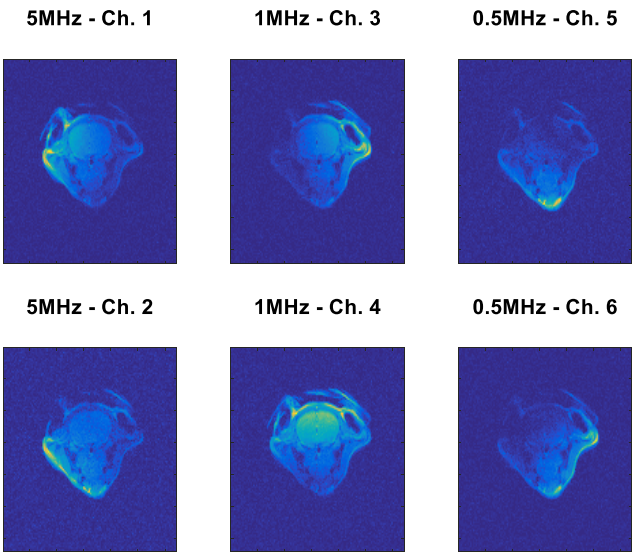

Figure 21: Images obtained of a live mouse brain from all 6 of the receive coils

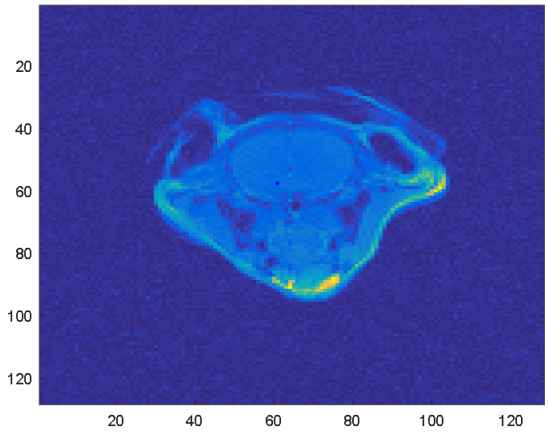

Figure 22: Combined image of mouse brain using sum of squares method

V.2 ^{1}H Imaging of 20 mM Phosphoric Acid Muscle Phantom on 3T Clinical Scanner

Experiments with the custom-made coil and corresponding connector were performed on the 3T Siemens Verio scanner at TIPS. For feasibility, only images were acquired. A phantom was utilized which is meant to mimic the phosphocreatine levels that may be expected in human muscle tissue (20 mM). Seen below in Figure 23 is the phantom on top of the custom coil. The same phantom was utilized with the larger commercial coil as well. A large phantom was chosen to exemplify that the larger commercial coil would be able to penetrate deeper into the phantom as compared with the smaller custom-made coil.

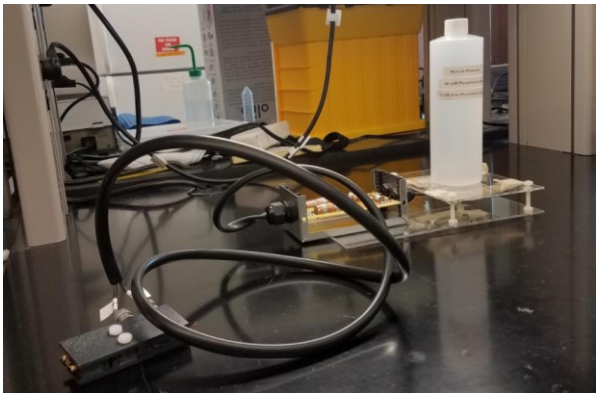

Figure 23: Connector, custom coil, and phantom together as within the imaging bore

Three images are shown below in Figure 24: the first (left) acquired using the commercial coil, the second (middle) using the custom coil but with no power adjustment, and the third (right) using the custom coil but with the power reduced:

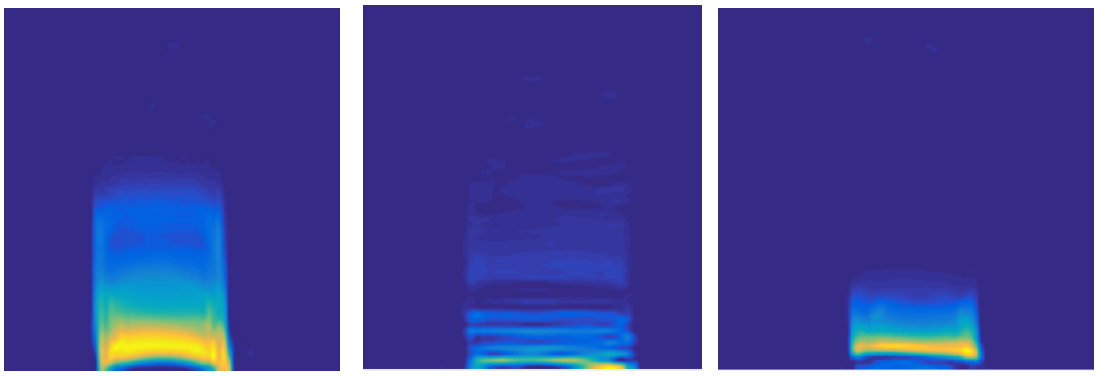

Figure 24: Presentation of the images acquired with: the commercial coil on the left, the custom coil with unchanged power requirements in the middle, and the custom coil with adjusted power levels on the right

It can be seen that the larger coil is able to penetrate deeper into the phantom. This is due to the nature of the magnetic field produced by the butterfly coil. Since the coil is physically larger, the magnetic field that it produces will also be at a larger depth above the coil compared to the smaller custom coil. The custom coil will therefore

produce a magnetic field that does not penetrate as deeply as the larger coil. The striated bands seen in the middle photo represent over-tipping, which is occurring wherever the spins are being tipped 180 degrees, effectively nulling the signal from these areas.

Next, the signal-to-noise ratio (SNR) was compared between the commercial coil and the custom coil through calculating the average signal level where the signal is most uniform near the coil and then dividing that by the standard deviation of the noise. Where exactly the signal and the noise measurements were extracted from can be seen by the rectangles within the images within Figure 25. The respective signal and noise values calculated are found in Table 3.

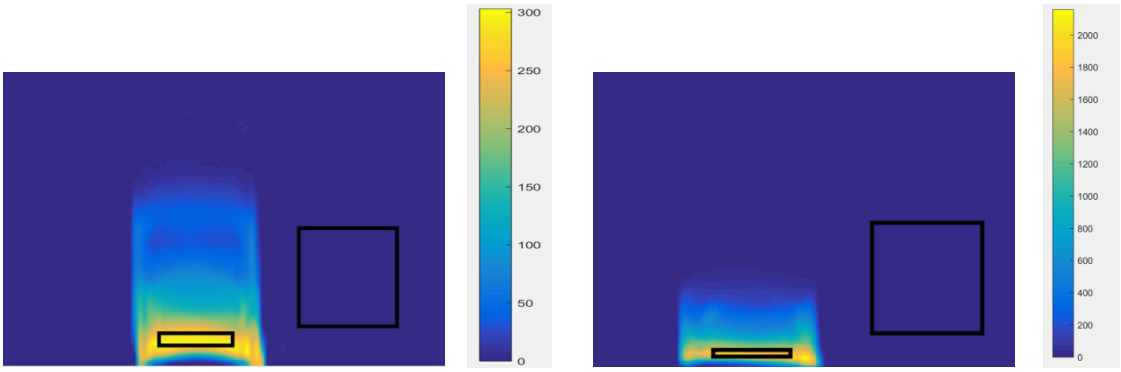

Figure 25: Demonstrating signal intensities and where the signal and noise regions are calculated

Table 3: SNR comparison between commercial and custom coil

Coil	Signal	Noise	SNR
Commercial	286.44	$1.8782*10^{-6}$	$1.5251*10^{8}$
Custom	1794.45	$1.6968*10^{-6}$	$1.0575*10^{9}$

$$\frac{SNR_{Custom}}{SNR_{Commercial}} = 6.93$$

Note the unusually high SNR values obtained are thought to be due to additional post-processing that is being performed on the images by the Siemens system. While the values themselves are unreasonable, the SNR is still able to be compared between the two coils. As discussed, the smaller coil does not pick up as much noise as the larger coil while imaging a region of interest similar in size to the smaller coil. The custom coil then has an SNR approximately 7 times that of the larger commercial coil. This confirms was what previously thought in that building the smaller coil would produce a higher SNR, which will be necessary once performing ^{31}P spectroscopy.

CHAPTER VI:

CONCLUSIONS AND FUTURE WORK

DMD is a debilitating disease with no currently available cure, resulting in death of the males who have the disease occurring in their 20's due to respiratory and cardiac complications. A treatment therefore needs to be found. While there are a few different ways of evaluating treatment outcomes of the disease such as muscle biopsy, MRI, and MRS, MRS is thought to be the best option due to its non-invasiveness and its ability to quantify metabolites locally.

While ^{1}H spectroscopy may be performed in order detect lipid concentrations within a muscle of interest, a full "tissue signature" regarding cellular and muscular activity is thought to be necessary to form a biomarker of the disease, requiring additional nuclei spectra such as ^{31}P to be acquired. Such secondary-nuclei have lower sensitivities than ^{1}H, and therefore require means of increasing the sensitivity. Two methods are discussed within this research which lead to higher sensitivity: increasing the number of RF coils and optimizing the coil size to the region of interest.

Both projects of this work integrate external hardware on existing systems with the intention of increasing the sensitivity of multinuclear studies to further the research capabilities of evaluating muscular dystrophy *in vivo* through MRS applications. While no MRS experiments were performed directly, the experiments and their results prove the effectiveness of this work with the intention that the future steps in these projects will involve the acquisition of spectra.

For the receiver, in future experiments the improved user interface and calibration capability will allow for spectra to be acquired much easier than previously possible, and the added calibration functionality will ensure that the maximum sensitivity is achieved. For the connector and subsequent custom coil, images were acquired proving the expected increase in SNR as compared to the larger commercial coil. The next step will involve acquiring ^{31}P spectra on the 3T commercial scanner using the custom coil and connector.

Both of these projects ultimately work towards finding a cure for DMD, and it is my sincere hope that they prove worthwhile in doing so for the benefit of all of those affected by this disease.

REFERENCES

1. 2002; Available from: http://chemistry.umeche.maine.edu/CHY431/NMR/NMR-4.html.

2. Ackerman, J.J.H., *Mapping of metabolites in whole animals by 31P NMR using surface coils.* Nature, 1980. **283**(5743): p. 167-170.

3. Obert, D., et al., *Brain Metabolite Changes in Patients with Relapsing-Remitting and Secondary Progressive Multiple Sclerosis: A Two-Year Follow-Up Study.* PLoS ONE, 2016. **11**(9): p. 1-15.

4. Newman, R.J., et al., *Nuclear Magnetic Resonance Studies Of Forearm Muscle In Duchenne Dystrophy*. 1982, British Medical Association. p. 1072.

5. McDougall, M.P., et al., *Quadrature Transmit Coil for Breast Imaging at 7 Tesla Using Forced Current Excitation for Improved Homogeneity.* JOURNAL OF MAGNETIC RESONANCE IMAGING, 2014. **40**(5): p. 1165-1173.

6. Cui, W., et al., *Early Detection of Myocardial Bioenergetic Deficits: A 9.4 Tesla Complete Non Invasive 31P MR Spectroscopy Study in Mice with Muscular Dystrophy.* Plos One, 2015. **10**(8): p. e0135000-e0135000.

7. Kornegay, J.N., et al., *Pharmacologic Management of Duchenne Muscular Dystrophy: Target Identification and Preclinical Trials.* ILAR JOURNAL, 2014. **55**(1): p. 119-149.

8. Bushby, K., *Review: Diagnosis and management of Duchenne muscular dystrophy, part 1: diagnosis, and pharmacological and psychosocial management.* The Lancet Neurology, 2010. **9**(1): p. 77-93.

9. Hayashita-Kinoh, H., et al., *Intra-amniotic rAAV-mediated microdystrophin gene transfer improves canine X-linked muscular dystrophy and may induce immune tolerance.* Molecular Therapy: The Journal Of The American Society Of Gene Therapy, 2015. **23**(4): p. 627-637.

10. Finanger, E.L., et al., *Use of skeletal muscle MRI in diagnosis and monitoring disease progression in Duchenne Muscular Dystrophy.* Physical Medicine & Rehabilitation Clinics of North America, 2011.

11. Thibaud, J.L., et al., *Characterization of dystrophic muscle in golden retriever muscular dystrophy dogs by nuclear magnetic resonance imaging.* Neuromuscular Disorders, 2007. **17**: p. 575-584.

12. Monforte, M., *Calf muscle involvement in Becker muscular dystrophy: When size does not matter.* Journal of the neurological sciences, 2014. **347**(1-2): p. 301-304.

13. Arpan, I., *Examination of effects of corticosteroids on skeletal muscles of boys with DMD using MRI and MRS.* Neurology, 2014. **83**(11): p. 974-980.

14. Kushnir, T., et al., *In vivo 23Na NMR studies of myotonic dystrophy.* Magnetic resonance in medicine, 1997. **37**(2): p. 192-196.

15. Stapleton, D.I., et al., *Dysfunctional muscle and liver glycogen metabolism in mdx dystrophic mice.* Plos One, 2014. **9**(3): p. e91514-e91514.

16. Falzarano, M.S., et al., *Duchenne Muscular Dystrophy: From Diagnosis to Therapy.* Molecules, 2015. **20**(10): p. 18168-18184.

17. Petrof, B.J., *The molecular basis of activity-induced muscle injury in Duchenne muscular dystrophy.* Molecular And Cellular Biochemistry, 1998. **179**(1-2): p. 111-123.

18. Beytía, M.d.l.A., J. Vry, and J. Kirschner, *Drug treatment of Duchenne muscular dystrophy: available evidence and perspectives.* Acta Myologica: Myopathies And Cardiomyopathies: Official Journal Of The Mediterranean Society Of Myology / Edited By The Gaetano Conte Academy For The Study Of Striated Muscle Diseases, 2012. **31**(1): p. 4-8.

19. Nakamura, A. and S.i. Takeda, *Mammalian models of Duchenne Muscular Dystrophy: pathological characteristics and therapeutic applications.* Journal Of Biomedicine & Biotechnology, 2011. **2011**: p. 184393-184393.

20. Valentine, B.A., B.J. Cummings Jf Fau - Cooper, and B.J. Cooper, *Development of Duchenne-type cardiomyopathy. Morphologic studies in a canine model.* (0002-9440 (Print)).

21. Kornegay, J.N., et al., *Golden retriever muscular dystrophy (GRMD): Developing and maintaining a colony and physiological functional measurements.* Methods in molecular biology (Clifton, N.J.), 2011. **709**: p. 105-123.

22. Acosta, A.R., et al., *Use of the six-minute walk test to characterize golden retriever muscular dystrophy.* Neuromuscular Disorders, 2016. **26**: p. 865-872.

23. *Chem LibreTexts*. 2017.

24. *Chapter 2: Principles of Magnetic Resonance Imaging*. Available from: https://users.fmrib.ox.ac.uk/~stuart/thesis/chapter_2/chapter2.html.

25. Macomber, R.S., *A Complete Introduction to Modern NMR Spectroscopy*. 1998: Wiley.

26. *NMR and MRI: Applications in Chemistry and Medicine.* 2011.

27. Kemp, G.J., *Cellular energetics of dystrophic muscle.* Journal of the neurological sciences, 1993. **116**(2): p. 201-206.

28. Wary, C., et al., *Splitting of Pi and other ³¹P NMR anomalies of skeletal muscle metabolites in canine muscular dystrophy.* NMR In Biomedicine, 2012. **25**(10): p. 1160-1169.

29. McCully, K., *Canine X-linked muscular dystrophy studied with in vivo phosphorus magnetic resonance spectroscopy.* Muscle & nerve, 1991. **14**(11): p. 1091-8.

30. Dabirzadeh, A., *Rf coil design for multi-frequency magnetic resonance imaging & spectroscopy*, in *Electrical Engineering*. 2008, Texas A&M Engineering.

31. Asher, K., et al., *Radiofrequency Coils for Musculoskeletal MRI.* Topics in magnetic resonance imaging : TMRI, 2010. **21**(5): p. 315-323.

32. Chiang, W.-Y., *Streamlining the Design and Use of Array Coils for In-Vivo Magnetic Resonance Imaging of Small Animals*, in *Biomedical Engineering*. 2016, Texas A&M University.

33. Eigenbrodt, E., *Multi-Channel, Frequency-Agnostic, Portable Receiver Design for Magnetic Resonance Imaging and Spectroscopy*, in *Electrical Engineering*. 2016, Texas A&M University.

34. Sia, J., *DEVELOPMENT OF A 1H/31P SPECTROSCOPY COIL CUSTOMIZED FOR CANINE MODELS OF MUSCULAR DYSTROPHY*, in *Biomedical Engineering*. 2016, Texas A&M University.

35. Arthur W. Magill, R.G., *Nested Surface Coils for Multinuclear NMR*, in *RF Coils for MRI*, J.R.G. J. Thomas Vaughan, Editor. 2012, Wiley.